JGR Atmospheres

RESEARCH ARTICLE
10.1029/2020JD032674

Assessment of Uncertainty Sources in Snow Cover Simulation in the Tibetan Plateau

Yingsha Jiang[1], Fei Chen[2], Yanhong Gao[3], Cenlin He[2], Michael Barlage[2], and Wubin Huang[4]

[1]Key Laboratory of Land Surface Process and Climate Change in Cold and Arid Regions, Northwest Institute of Eco-Environment and Resources, Chinese Academy of Sciences, Lanzhou, China, [2]Research Applications Laboratory, National Center for Atmospheric Research, Boulder, CO, USA, [3]Department of Atmospheric and Oceanic Sciences and Institute of Atmospheric Sciences, Fudan University, Shanghai, China, [4]Lanzhou Central Meteorological Observatory, Lanzhou, China

Abstract Snow cover over the Tibetan Plateau (TP) plays an important role in Asian climate. State-of-the-art models, however, show significant simulation biases. In this study, we assess the main uncertainty associated with model physics in snow cover modeling over the TP using ground-based observations and high-resolution snow cover satellite products from the Moderate Resolution Imaging Spectroradiometer (MODIS) and FengYun-3B (FY3B). We first conducted 10-km simulations using the Noah with multiparameterization (Noah-MP) land surface model by optimizing physics-scheme options, which reduces 8.2% absolute bias of annual snow cover fraction (SCF) compared with the default model settings. Then, five SCF parameterizations in Noah-MP were optimized and assessed, with three of them further reducing the annual SCF biases from around 15% to less than 2%. Thus, optimizing SCF parameterizations appears to be more important than optimizing physics-scheme options in reducing the uncertainty of snow modeling. As a result of improved SCF, the positive bias of simulated surface albedo decreases significantly compared to the GLASS albedo data, particularly in high-elevation regions. This substantially enhances the absorbed solar radiation and further reduces the annual mean biases of ground temperature from −3.5 to −0.8°C and snow depth from 4.2 to 0.2 mm. However, the optimized model still overestimates SCF in the western TP and underestimates SCF in the eastern TP. Further analysis using a higher-resolution (4 km) simulation driven by topographically adjusted air temperature shows slight improvement, suggesting a rather limited contribution of the finer-scale land surface characteristics to SCF uncertainty.

Key Points:
- Optimizing Noah-MP physics-scheme options reduces about 8% absolute bias of the annual snow cover fraction (SCF) compared to MODIS SCF
- Optimizing SCF parameterizations further reduces around 13% SCF absolute bias, which is higher than optimizing physics-scheme options
- Contributions of high-resolution topographically adjusted air temperature to the SCF simulation uncertainty are limited

Supporting Information:
- Supporting Information S1

Correspondence to:
Y. Gao,
gaoyh@fudan.edu.cn

Citation:
Jiang, Y., Chen, F., Gao, Y., He, C., Barlage, M., & Huang, W. (2020). Assessment of uncertainty sources in snow cover simulation in the Tibetan plateau. *Journal of Geophysical Research: Atmospheres*, *125*, e2020JD032674. https://doi.org/10.1029/2020JD032674

Received 27 FEB 2020
Accepted 30 AUG 2020
Accepted article online 4 SEP 2020

1. Introduction

Snow cover significantly affects surface energy budget and heat fluxes by reducing surface absorption of solar radiation due to its high albedo and low thermal conductivity and, hence, influences regional and global climate through the land-atmosphere interactions (Chen et al., 2014; Clark & Serreze, 2000; Steger et al., 2013; Xu & Dirmeyer, 2011; Xue, 2003). As the "Third Pole," the Tibetan Plateau (TP) possesses the largest amount of snow and glacier in the midlatitudes, which shows remarkable changes under the warming climate, such as glacier retreat and snow cover variations (Kang et al., 2010; Yao et al., 2019). More importantly, snow cover over the TP plays a unique role in Asian climate and its hydrological system by affecting the occurrence and strength of Asian monsoon and precipitation (Gao et al., 2016; Immerzeel et al., 2010; Li et al., 2018; Liu & Yanai, 2002; Vernekar et al., 1995; Wang et al., 2018; Wu et al., 2007, 2012; Zhang et al., 2004). Therefore, it is important to accurately simulate snow cover over the TP in weather and climate models.

Previous studies found that land and climate models with proper configurations could reasonably reproduce snow cover in most areas of the Northern Hemisphere but are problematic for complex-terrain areas. For example, Barlage et al. (2010) and Livneh et al. (2010) found negative biases of snow depth and snow water equivalent for the Noah land surface model (LSM) in the Rocky mountain areas of the western United States. In the French mountains, positive biases of snowpack for the regional model and CROCUS snow model were found (Quéno et al., 2016; Vionnet et al., 2016, 2019). He et al. (2019) found systematic positive biases in snow cover fraction (SCF) and surface albedo in the western United States using five precipitation data

Table 1

SCF Parameterizations and Their Optimized Versions, Where d Is Snow Depth (m), z_0 Is Surface Roughness Length ($z_0 = 0.01$ m, But It Is Set to 0.002 m for HRLDAS Version 3.9), Sn Is Snow Water Equivalent (kg/m^2), ρ_s Is Snow Density, ρ_{snew} Is the Snow Density for New Snow Fall, m Is the Melting Factor ($m = 2.5$ for the Original N07 in HRLDAS and $m = 1.6$ for the Optimized N07)

	References	Original equations	Optimized equations
D81	Dickinson et al. (1986)	$\mathrm{SCF} = \frac{d}{(10z_0 + d)}$	$\mathrm{SCF} = \frac{d}{(z_0 + d)}$
Y97	Yang et al. (1997)	$\mathrm{SCF} = \tanh\left(\frac{d}{2.5z_0}\right)$	$\mathrm{SCF} = \tanh\left(\frac{d}{0.8 \times 2.5z_0}\right)$
R01	Roesch et al. (2001)	$\mathrm{SCF} = 0.95\tanh(100\mathrm{Sn})$	$\mathrm{SCF} = 0.8\tanh(100\mathrm{Sn})$
RT04	Romanov and Tarpley (2004)	$\mathrm{SCF} = \ln(d+1)/3.33$	$\mathrm{SCF} = \ln(100d+1)/2$
N07	Niu and Yang (2007)	$\mathrm{SCF} = \tanh\left(\frac{d}{2.5z_0\left(\frac{\rho_s}{\rho_{snew}}\right)^m}\right)$	$\mathrm{SCF} = \tanh\left(\frac{d}{0.8 \times 2.5z_0\left(\frac{\rho_s}{\rho_{snew}}\right)^m}\right)$

sets as forcing data and pointed out the urgent need to improve snowpack physics. For the TP area, Orsolini et al. (2019) found systematic overestimates of snow depth and snow cover in various reanalysis products, including the European Center for Medium-Range Weather Forecasts (ECMWF) ERA5 and ERA-Interim data sets, the Japanese 55-year Reanalysis (JRA-55), and the NASA Modern-Era Retrospective analysis for Research and Applications (MERRA-2). Toure et al. (2016) and Xie et al. (2018) found that the SCF is significantly overestimated in the TP using the Community Land Model (CLM) versions 4 and 4.5, respectively, compared with satellite observations. Xia et al. (2014) also pointed out that the overestimated SCF and snow depth over the TP are common problems based on the two climate models used. Moreover, we found that snow cover satellite data sets contain notable uncertainties over the TP (Jiang et al., 2019), such as the overestimate of the Interactive Multisensor Snow and Ice Mapping System (IMS) SCF product used by Xie et al. (2018), suggesting that the positive bias of the simulated SCF in the TP might be underestimated. The overestimated SCF will eventually change the surface energy budget in the model and result in high uncertainties in land-atmosphere interactions, which then affect simulations of Asian monsoon in spring (Wu & Qian, 2003). Thus, it is imperative to improve the SCF simulation in the TP.

Model physics and parameterizations of snow processes are major uncertainty sources in snow simulation (C. He et al., 2019; Chen et al., 2014). Previous studies have developed and evaluated a number of SCF parameterizations in land surface models. At the early stage, Dickinson et al. (1986) developed a parameterization (hereinafter the D81 formulation; see Table 1) in the Biosphere-Atmosphere Transfer Scheme (BATS) (Dickinson et al., 1986). A similar parameterization was used in the Météo-France climate model, but it adopted snow water equivalent (SWE) instead of snow depth as a variant (Donville et al., 1995). Later on, Yang et al. (1997) developed a new scheme (hereinafter the Y97 formulation; see Table 1) based on in situ observations in Russia, which was used in the CLM versions 2 and 3. Then, Niu and Yang (2007) improved the Y97 SCF parameterization by introducing SCF dependence on snow density (hereinafter the N07 formulation; see Table 1), which was constrained by satellite data of SCF and in situ observations of snow depth in North America. The N07 scheme has been widely used in land surface models, such as the CLM4, CLM4.5, and the Noah with multiparameterization (Noah-MP), but its applications revealed significantly overestimated SCF in the TP (Xie et al., 2018). CLM5 applied a new SCF parameterization developed by Swenson and Lawrence (2012), but preliminary test in the TP showed that this scheme did not give substantially improvements compared to the N07 scheme (Xie et al., 2018).

In addition, Luce et al. (1999) and Liston (2004) developed a subgrid snow distribution model based on station observations, which calculates SCF as a function of snowmelt amount. Roesch et al. (2001) developed three SCF formulas suitable for three topographic types in the ECHAM4 (hereinafter the R01 formulation; see Table 1). Romanov and Tarpley (2004) developed a relationship between SCF and snow depth (hereinafter the RT04 formulation; see Table 1) based on in situ observations of snow depth and satellite retrievals of SCF in the Great Plains of the United States and Canada. However, the preceding SCF schemes were mainly developed and tested in North America or Russia, where snow cover is relatively thick and extensive, which could be problematic for the TP with relatively thin and short-lived snow (shown in Figure 1) and

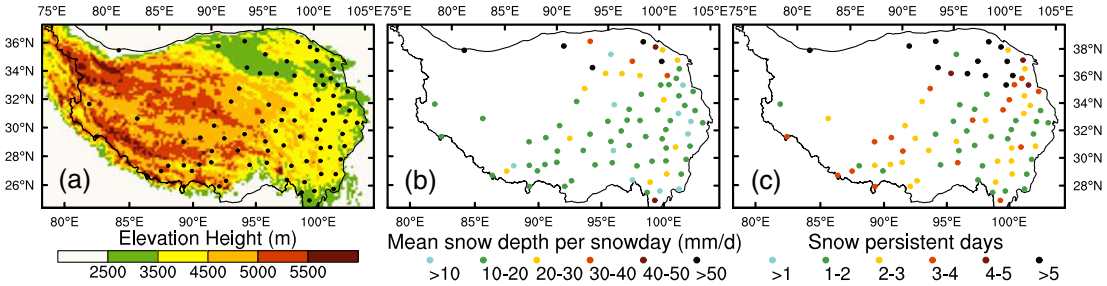

Figure 1. The elevation (m) of the study area and the locations of in situ observation stations in the TP (a), mean snow depth per snow day (b; mm/day), and annual-mean snow persistent days (c) from in situ observations in 2010–2015.

might result in large cold biases of surface air temperature over the TP (Gao et al., 2018; Gao, Xu, et al., 2015; Gao & Chen, 2017).

Therefore, the main purpose of this study is to assess the uncertainty of model physics in multiscale-resolution snow cover simulations over the TP by optimizing physics-scheme options and parameterizations. This is a follow-up study of Jiang et al. (2019), which investigated the uncertainty in satellite snow cover data over the TP region. Descriptions of the study area and data sets, including station observations, satellite data sets, and gridded data used in the model, are provided in section 2. In section 3, we briefly introduce the Noah-MP LSM, model configurations, and optimizations. The Noah-MP is used here mainly because of its multiple physical schemes/options providing several parameterizations for each specific process of surface heat and water exchanges, which is appropriate for ensemble simulations and uncertainty analysis (Li et al., 2018; You et al., 2020; Zhang et al., 2016). Simulation results and improvements of snow cover modeling and uncertainty analysis are provided in section 4. In section 5, we briefly discuss the uncertainty of forcing data in snow cover modeling in the TP. Conclusions are given in section 6.

2. Data Sets

2.1. Atmospheric Forcing and Land-Surface Data Sets

The atmospheric forcing data set used here is the China Meteorological Forcing Dataset (CMFD; https://data.tpdc.ac.cn/zh-hans/data/8028b944-daaa-4511-8769-965612652c49/; He et al., 2020). It combines a variety of data sets, including the China Meteorological Administration (CMA) station observations, the Global Land Data Assimilation System data, the Princeton forcing data, the Tropical Rainfall Measurement Mission (TRMM 3B42) precipitation, and the downward shortwave radiation from the Global Energy and Water Cycle Experiment-Surface Radiation Budget (He et al., 2020). The 0.1°, 3-hourly data set covers China for the period from 1979 to 2015 and provides seven forcing variables, including surface air temperature, surface pressure, specific humidity, wind speed, precipitation, and downward shortwave and longwave radiation. Six of them (not including downward shortwave radiation) were further interpolated into hourly resolution using the Piecewise Cubic Hermite Interpolating Polynomial method (Birkhoff & De Boor, 1965), and the downward shortwave radiation was interpolated with the effects of solar elevation angle.

MODIS 0.1° multiyear mean (2001–2012) monthly leaf area index (LAI) data and MODIS/Terra+Aqua Land Cover Type Yearly L3 Global 500 m data (MCD12Q1; http://doi.org/10.5067/MODIS/MCD12Q1.006) were used to replace the Noah-MP model default vegetation parameters. The 0.0083° Chinese Dataset of Soil Hydraulic Parameters Using Pedotransfer Functions for Land Surface Modeling (Dai et al., 2013) was used to specify soil properties, such as the amount of soil sand/clay content and organic matter.

2.2. Model Validation Data Sets

We used both *in-situ* observations and satellite data sets to evaluate model results. *In-situ* observations of snow depth and ground temperature (at the surface) in 2010–2015 are from the CMA and the National Meteorological Information Center (http://data.cma.cn/site/index.html; Figure 1a). Observations of snow depth show that the majority stations in the TP have snow depths less than 30 mm per snow day, and the duration of snow is usually shorter than 5 days (Figures 1b and 1c). However, only 83 stations are located in the TP, and most of them are in the eastern regions, with no stations at elevation higher than 4,800 m

(Figure 1a; Gao et al., 2018). Thus, it is necessary to use satellite data with high temporal and spatial resolution to capture the fast snow cover change over the high elevation with complex terrain.

Based on our previous evaluations (Jiang et al., 2019), two spatiotemporally high-resolution satellite data sets of SCF from the FengYun-3B (FY3B) and the Moderate Resolution Imaging Spectroradiometer (MODIS) were used in this study. FY3B is one of the Chinese FengYun-3 (FY3) second-generation polar-orbiting meteorological satellites (Dong et al., 2009), providing multisensor synergy (MULSS) daily snow cover product at 0.01° resolution from 2012 to the present (http://satellite.nsmc.org.cn/PortalSite/Data/Satellite.aspx). MODIS is a 36-channel visible thermal-infrared sensor of the NASA Earth Observation System (EOS) (Hall et al., 2002). Daily 500-m snow cover products version 6 in 2011–2017 of two MODIS sensors, Terra and Aqua (MOD10A1, https://nsidc.org/data/mod10a1; MYD10A1, https://nsidc.org/data/myd10a1), were merged to remove clouds first. Then, a four-step cloud-removal procedure was applied to the merged MODIS data and the FY3B, which reduced the cloud percentage from around 45% to 3% for both data sets (Jiang et al., 2019). Finally, two data sets were converted to the same resolution of 0.04°. Evaluation results of the satellite SCF data show a classification accuracy of about 94% for the FY3B data, which is higher than the 0.04° MODIS and Multisensor Snow and IMS (Jiang et al., 2019). Therefore, we selected the FY3B data due to its high accuracy and the MODIS data due to its wide application as the observations of SCF in the TP. FY3B and MODIS SCF have more consistent climatology and interannual changes than IMS as well. Despite this, SCF extracted from any single data set at individual grids can have large uncertainties with extreme or unreasonable values. Thus, we used the ensemble mean of FY3B and MODIS data when extracting SCF for observation stations in sections 3.3 and 4.1 For the spatial distribution analysis of SCF in section 4, FY3B and MODIS data are used separately.

We also used satellite surface albedo data of the GLASS product (GLASS02B05) developed by the National Earth System Science Data Center, National Science and Technology Infrastructure of China (http://www.geodata.cn). This 5-km, 8-day data set provides the black-sky albedo and white-sky albedo in shortwave, visible, and near infrared bands, respectively. Here we used the albedo data in the shortwave band. The ground albedo (α) is derived by a function using the black-sky albedo (α_{bsa}), white-sky albedo (α_{wsa}), and the diffuse skylight fraction (S; Text S1 in the supporting information) (Lewis & Barnsley, 1994; Lucht et al., 2000; Ma et al., 2019; Wang et al., 2004).

$$\alpha = (1 - \mathrm{S}) \times \alpha_{bsa} + \mathrm{S} \times \alpha_{wsa} \tag{1}$$

This albedo data set is valid at local noontime and has a processing window of 17 days for the 8-day value, which means the albedo of i day is actually the average value from $i - 8$ to $i + 8$ days. Thus, we extracted and generated the albedo data of simulation results in the same way, to be consistent with the GLASS data.

3. Methods

3.1. Model Descriptions

The LSM used in this study is the Noah-MP (Niu et al., 2011; Yang et al., 2011), coupled with the High Resolution Land Data Assimilation System (HRLDAS; Chen et al., 2007) version 3.9 (https://ral.ucar.edu/solutions/products/high-resolution-land-data-assimilation-system-hrldas). Noah-MP is widely used in climate and hydrology modeling because of its comprehensive physical processes of land surface evolution and heat and hydro exchanges (Barlage et al., 2015; Gao et al., 2016). A significant advantage of Noah-MP is its multiple physical schemes/options; it provides several parameterizations for each specific process for surface heat and water exchanges (Zhang et al., 2016). The physical processes with multiple options include the surface-layer exchange coefficient (SFC), runoff and groundwater (RUN), canopy stomatal resistance (CSR), soil moisture factor for stomatal resistance (BTR), snow albedo (SA), surface resistance (SRE), rain-snow partitioning (PCP), and snow/soil temperature time scheme (TEMT), as shown in Table 2. Other physical processes include dynamic vegetation, frozen soil permeability, and canopy radiative transfer.

Previous evaluations of Noah-MP in the TP showed that it can reproduce reasonably well the key land-surface processes (e.g., soil temperature and moisture, surface latent, and sensible heat fluxes) of the

Table 2
Physical Processes With Multiple Options in the Noah-MP, Which Were Used in the Sensitivity Tests in Section 4.1 and the Options Applied in the Controlled Simulation (CTL) and the Simulation With Optimized Physics-Scheme Options (OPT)

Physical processes	Options	CTL	OPT
Canopy Stomatal Resistance (CSR)	(1) Ball-Berry (2) Jarvis	(1)	(1)
Soil Moisture Factor for Stomatal Resistance (BTR)	(1) Noah (2) CLM	(1)	(1)
Runoff and Groundwater (RUN)	(1) SIMGM (2) SIMTOP (3) Noah (free drainage) (4) BATS (free drainage)	(2)	(2)
Surface-Layer Exchange Coefficient (SFC)	(1) Monin-Obukhov scheme (2) Noah (Chen97)	(1)	(2)
Snow Surface Albedo (SA)	(1) BATS (2) CLASS	(2)	(2)
Partitioning Precipitation into Rain/Snow (PCP)	(1) Jordan (2) BATS (3) SFCTMP (4) WRF microphysics output	(1)	(1)
Snow/Soil Temperature Time Scheme (TEMT)	(1) Semi-implicit (2) Full implicit (Noah) (3) Same as (1) but use SCF for surface temperature	(1)	(1)
Surface Resistance for Evaporation/Sublimation (SRE)	(1) Sakaguchi and Zeng (for nonsnow) (2) Sellers (3) Adjusted sellers (4) Same as (1) but for snow	(1)	(4)

TP (Gao, Li, et al., 2015; Jiang et al., 2018; Zhang et al., 2016), but these studies mainly focused on warm monsoon seasons. For winter processes, Chen et al. (2014) evaluated snow cover and heat-flux simulation of six LSMs including Noah-MP in the Colorado River Headwaters region and found a better winter radiation feedback for Noah-MP though their SWE are similar. Minder et al. (2016) also found a better represented SCF by Noah-MP than by Noah LSM over the Rocky Mountains. Among variables simulated by Noah-MP, SCF and net radiation show better performances than the others including the gross primary productivity and evapotranspiration (Ma et al., 2017). Thus, Noah-MP is appropriate for the simulations of winter processes over the TP.

3.2. Model Configurations

The simulations are conducted in a 10-km modeling domain covering the TP (75–105°E, 25–40°N) from 1 January 2012 to 31 December 2015, which is the overlapping period of the CMFD forcing data and satellite SCF data. The physical schemes of the controlled simulation (CTL) follows the work of Gao, Xu, et al. (2015) and Jiang et al. (2018), as shown in Table 2. The options of other physical processes used in this study include option 4 (table LAI with maximum vegetation fraction) for dynamic vegetation process, option 1 (no iteration) for supercool liquid water process, option 2 (nonlinear effects, less permeable) for frozen soil permeability process, option 3 (two-stream applied to vegetated fraction) for radiative transfer process, and option 1 (semi-implicit) for lower boundary condition of soil temperature process.

A higher-resolution (4 km) simulation was also conducted in the TP from 1 September 2013 to 31 August 2014. Forcing data of 4-km grid were interpolated from the 0.1° CMFD using bilinear interpolation. Furthermore, surface air temperature of 4-km forcing data was adjusted based on the elevation coefficient using lapse rate (Gao, Xu, et al., 2015), which is the decreasing rates of air temperature with increasing elevations in the nearest 9 × 9 grids of CMFD data.

To spin up land state variables, a 1-year Noah-MP simulation is usually repeated by 3 to 11 times depending on physics-scheme options (Chen et al., 2014; Gao, Li, et al., 2015; Jiang et al., 2018; Zhang et al., 2016). Here we used the 2011 CMFD data for spin-up and repeated five times according to our spin-up evaluation (supporting information Figure S1), which is also consistent with Li, Wang, and Huang (2018).

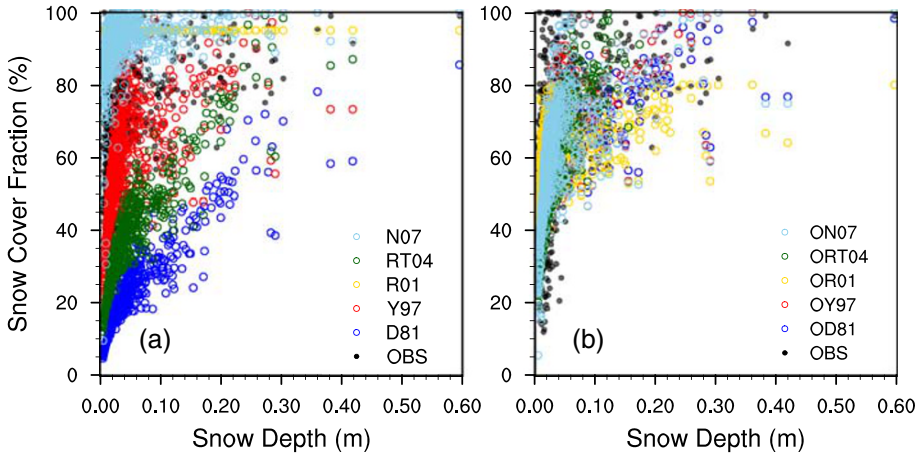

Figure 2. Scatterplots of snow depth (m) versus SCF (%). Snow depth is in situ observation. The SCF is from satellite data (black dots) and the five SCF parameterizations (color circles). (a) The SCF derived by using the original parameterizations and (b) the results after optimizations.

3.3. Optimizing SCF Parameterizations

Prior to spatial simulations, five SCF parameterizations (see Table 1) were evaluated offline using *in-situ* observations and satellite data. Here "offline" means using *in-situ* observed snow depth as input to the SCF parameterization in computing SCF, instead of running the full Noah-MP model. This method avoids uncertainties in modeling and forcing data in computing SCF but requires high-quality observations of snow depth and SCF. Among the 83 stations in the TP, 30 stations have total snow days less than 10 days in 6 years (2010–2015), so these stations are excluded. The snow density of N07 and SWE of R01 used here were calculated by the parameterization described in the supporting information (Text S2).

Figure 2a shows the relationships between snow depth and SCF derived from five parameterizations using snow depth observations as input. Y97 reproduces the observed (satellite) SCF better than the other schemes, with lower bias and root-mean-square error (RMSE; Table 3), but still overestimates the SCF even when using observed snow depth as input. This indicates that the current SCF parameterizations have systematic positive biases for SCF in the TP, which is consistent with the results over the western U.S. mountainous regions (He et al., 2019). Since we have daily high-accuracy and high-resolution observations in the TP, more accurate parameters in these five SCF parameterizations can be derived through fitting the observations in this area.

The curve-fitting toolbox (cftool) in MATLAB was used to find the appropriate parameters for the five parameterizations. It provides flexible regression analysis with various linear and nonlinear models, produces fitting equations with confidence intervals and residuals, and optimizes parameters for a specific formula. Therefore, the five SCF parameterizations were further optimized by using the optimized parameters derived from cftool, as shown in Table 1. This reduces the simulated SCF biases from over 20% to less than 6% for the stations and also decreases RMSE (Figure 2b), but only the optimized R01 and N07 have higher correlation coefficients (supporting information Table S1). Among the five modified parameterizations, the optimized Y97 has the best overall performance for ground observation stations, while the optimized RT04 and D81 have higher correlation coefficients (>0.4; supporting information Table S1).

4. Model Results and Uncertainty Analysis

4.1. Uncertainty From Multiple Physics-Scheme Options

Having multiple physics schemes is the main advantage of Noah-MP, but uncertainties can be introduced if inappropriate physics-scheme options are used. The physics-scheme options of CTL were mainly applied for warm seasons over the TP (Gao, Xu, et al., 2015). To test the sensitivity of the physics-scheme options on the SCF simulation in cold season, we conducted a number of sensitivity experiments with different physics-scheme options at the observation stations over the TP from 1 September 2013 to 31 August 2014.

Table 3
Annual Mean Biases (%), RMSE, and Pattern Correlation Between the MODIS SCF and Simulated SCF From the OPT With Original N07 and OPT With Five Optimized SCF Parameterizations (OPT/OD81 = OPT + the Optimized D81, OPT/OY97 = OPT + the Optimized Y97, OPT/OR01 = OPT + the Optimized R01, OPT/ORT04 = OPT + the Optimized RT04, and OPT/ON07 = OPT + the Optimized N07)

	OPT	OPT/ OD81	OPT/ OY97	OPT/ OR01	OPT/ ORT04	OPT/ ON07
Bias	14.6	1.8	5.6	15.1	1.89	0.9
RMSE	20.6	11.4	13.7	19.2	12.0	11.0
Corr.	0.69	0.76	0.76	0.74	0.76	0.76

Four schemes/processes (SA, PCP, TEMT, and SRE in Table 2) related to snow cover and four schemes (CSR, BTR, RUN, and SFC in Table 2) sensitive to land surface processes according to ensemble simulations (Zhang et al., 2016) were tested. First, eight physical schemes/processes were tested one by one while the other processes were kept unchanged. Then, for a specific scheme/process with multiple options, each option was applied in an individual simulation at the observation stations. Finally, we checked the biases of snow depth and SCF averaged in three seasons (spring, autumn, and winter) at the 83 observation stations in the TP.

Figure 3 shows no significant differences in biases of snow depth and SCF simulated by different options of CSR, BTR, RUN, and PCP schemes, which indicate a rather weak sensitivity of simulated snow cover and depth to these schemes/processes. The SFC scheme with option 2, the SA scheme with option 2, the TEMT scheme with option 1 or 3, and the SRE scheme with option 2, 3, or 4 (details in Table 2) have relatively smaller biases for both snow depth and SCF than the other options (Figure 3). The high sensitivity of SFC and TEMT scheme to the snow depth simulation in North Xinjiang, China was also reported by You et al. (2020). Therefore, we used option 2 of the SFC scheme and option 4 of the SRE scheme and kept the other schemes the same as those in CTL for simulations with the optimized physics-scheme options (OPT) shown in Table 2.

The OPT were then used in a 10-km simulation covering the whole TP in 2012–2015 to investigate their impact on regional snow cover simulation. Figure 4 shows that CTL significantly overestimates SCF in the TP compared to MODIS and FY3B, with annual mean biases over 20%, especially in the northwestern

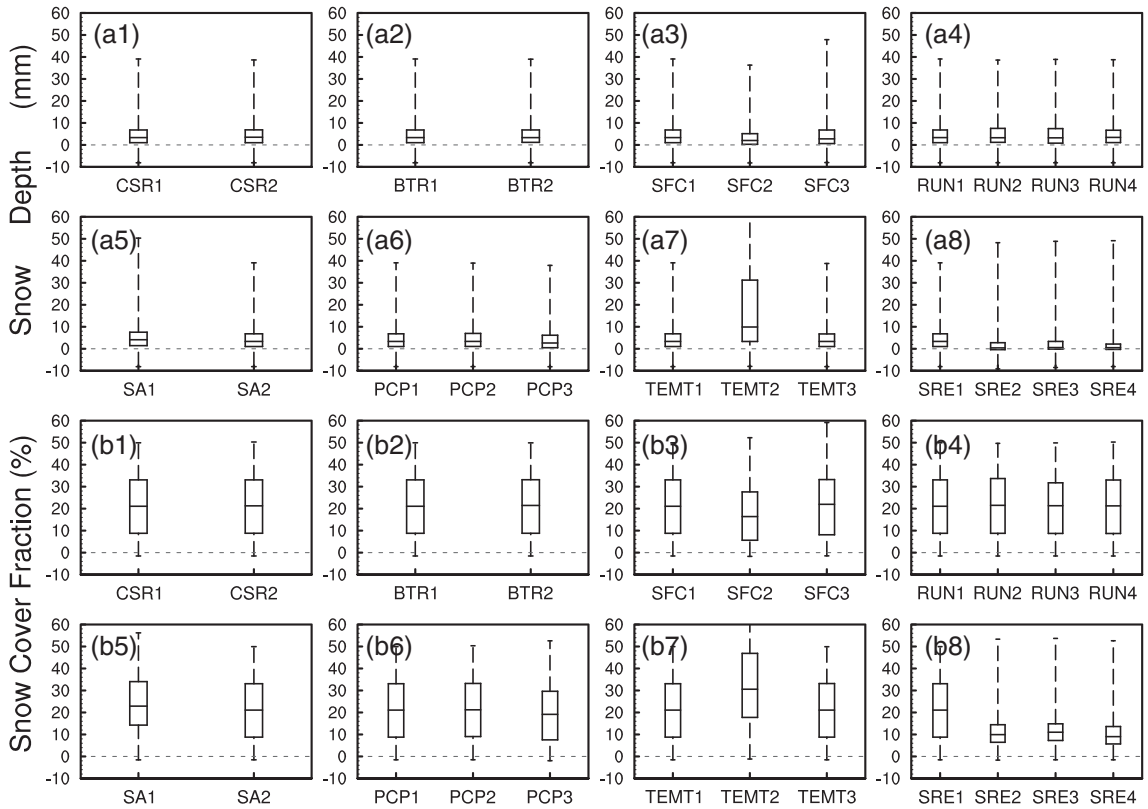

Figure 3. Box plots for the biases of snow depth (mm; a1–a8) and SCF (%; b1–b8) between observations and simulations from 1 September 2013 to 31 August 2014 using different physic-scheme options at the 83 stations in the TP. Eight physic schemes tested here are the CSR (a1, b1), BTR (a2, b2), SFC (a3, b3), RUN(a4, b4), SA(a5, b5), PCP(a6, b6), TEMT(a7, b7), and SRE(a8, b8).

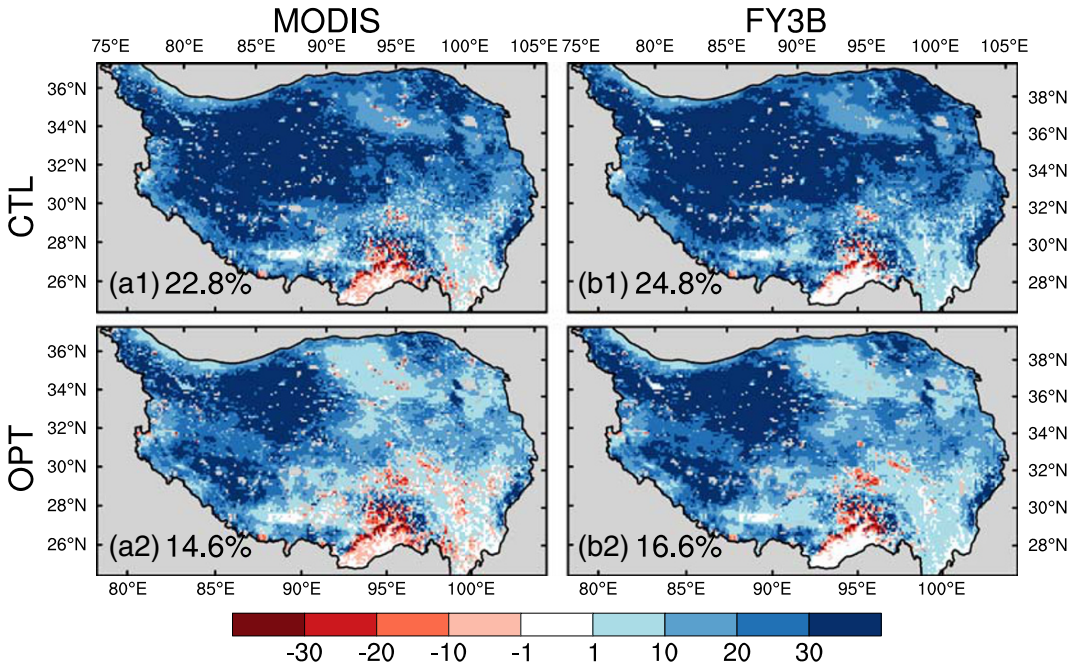

Figure 4. Biases of annual SCF (%) in 2012–2015 between MODIS/FY3B data and CTL/OPT simulation in the TP. Their spatial average values are given at the lower left corner.

regions. SCF biases in winter are even higher, which are over 50% and 60% compared to MODIS and FY3B, respectively. Compared to CTL, the OPT simulates the annual SCF more accurately, with annual mean biases reduced from 22.8% and 24.8% to 14.6% and 16.6% averaged over the TP compared to MODIS and FY3B data, respectively (Figures 4a2 and 4b2). Thus, the reduced absolute bias of annual SCF by using the OPT is about 8.2%, indicating that optimizing the Noah-MP physics-scheme options helps reduce the uncertainty in SCF simulation.

4.2. Uncertainty From SCF Parameterizations

Although the OPT improves SCF simulation, it still overestimates SCF significantly. The five optimized SCF parameterizations introduced in section 3.3 were then applied with the OPT in 10-km simulations covering the whole TP in 2012–2015. Figure 5 shows that compared to the MODIS data, the high positive bias of annual SCF of the OPT simulation is reduced significantly by using the optimized SCF parameterizations, except for optimized R01. Biases of annual SCF averaged over the TP reduce to around 1–2% for the OPT with optimized D81, RT04, and N07, which are lower than those with optimized Y97 and R01 (Table 3). Comparison with the FY3B data shows similar results (supporting information Figure S2). This suggests that SCF parameterizations contribute significantly to the uncertainty of SCF simulation in the TP, which appears to be more important than an optimized combination of physics-scheme options (section 4.1).

Among the five parameterizations, optimized N07 produces the lowest bias and RMSE with higher pattern correlation coefficient compared with satellite data (Table 3). Spatial mean daily SCF (supporting information Figure S3) shows that all the schemes can generally capture the seasonal variations of snow cover, but the OPT with optimized D81, RT04, or N07 generates better SCF values, which is mainly because optimized D81, RT04, and N07 reduce the SCF value in the early snow accumulation age.

However, the annual SCF of the OPT simulation with optimized parameterizations is still overestimated in the western TP and underestimated in the eastern TP especially in mountainous areas (Figure 5). Moreover, biases of annual SCF have generally similar spatial distributions for the OPT with optimized D81, RT04, and N07. This suggests that the remaining SCF uncertainties are likely related to the atmospheric forcing data (especially orographic precipitation for the southeastern TP area, as pointed out by Gao et al., 2020) and sub-grid scale topographic effects.

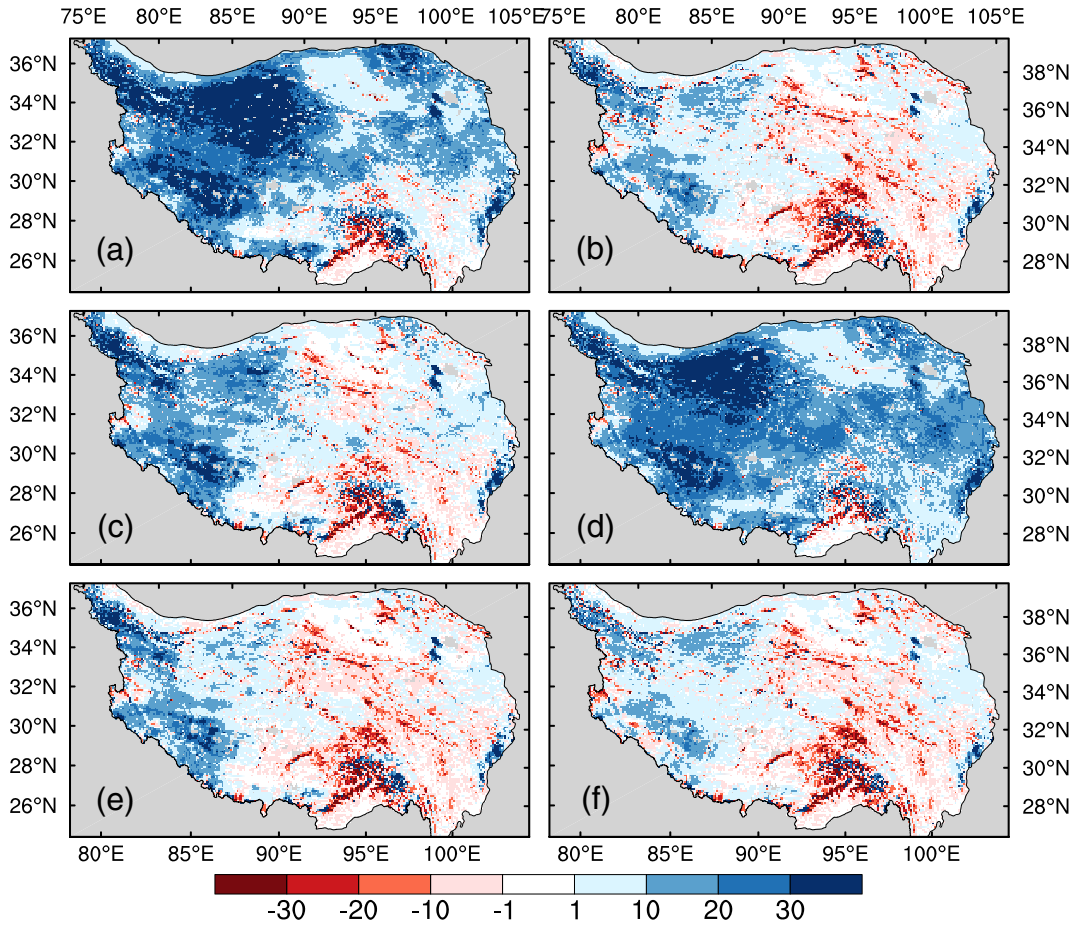

Figure 5. Annual-mean biases of SCF (%) in 2012–2015 of OPT simulation results using the original N07 (OPT; a), the optimized D81 (OPT/OD81; b), the optimized Y97 (OPT/OY97; c), the optimized R01 (OPT/OR01; d), the optimized RT04 (OPT/ORT04; e), and the optimized N07 (OPT/ON07; f), with respect to the MODIS snow cover data.

4.3. Uncertainty From Model Spatial Resolution

To explore the effects of scale dependency, a higher-resolution (4 km) simulation using the OPT and optimized N07 was conducted in the TP in a continuous snow season from 1 September 2013 to 31 August 2014.

Figure 6 shows the biases of annual SCF at 10- and 4-km resolutions compared to the MODIS and FY3B data. Generally, the spatial distribution of 4-km annual SCF shows slight improvements. Compared to the 10-km simulations, the negative SCF biases in the central to eastern TP are reduced by using the 4-km simulation, so are the positive SCF biases in the northwestern TP (Figure 6). Seasonal and annual biases of 4-km SCF are also lower than those of 10-km SCF, except for summer (Table 4). Spatial mean daily SCF (Figure 7) shows that both of the OPT/ON07 in 10- and 4-km resolutions can generally capture the seasonal variation of snow cover, which is closer to the MODIS data than CTL and other optimized SCF schemes. Furthermore, the 4-km OPT/ON07 has lower SCF in the early snow accumulation age than its 10-km resolution counterpart, while they are very close in the other periods. This is probably because the impacts of the adjusted air temperature of 4-km resolution mainly show in the snow accumulation period.

However, the negative SCF biases on top of the mountains are more significant in the 4-km simulation than in the 10 km one, such as the Qilian Mountain region in the northeastern TP (Figure 6). This suggests that higher spatial resolution does not solve the main problem of SCF biases in high mountains of the TP. Thus, the uncertainty from using different model spatial resolutions tends to be small in this study. This is mainly because no significant differences exist in the forcing data for the two simulations except for the adjusted air temperature.

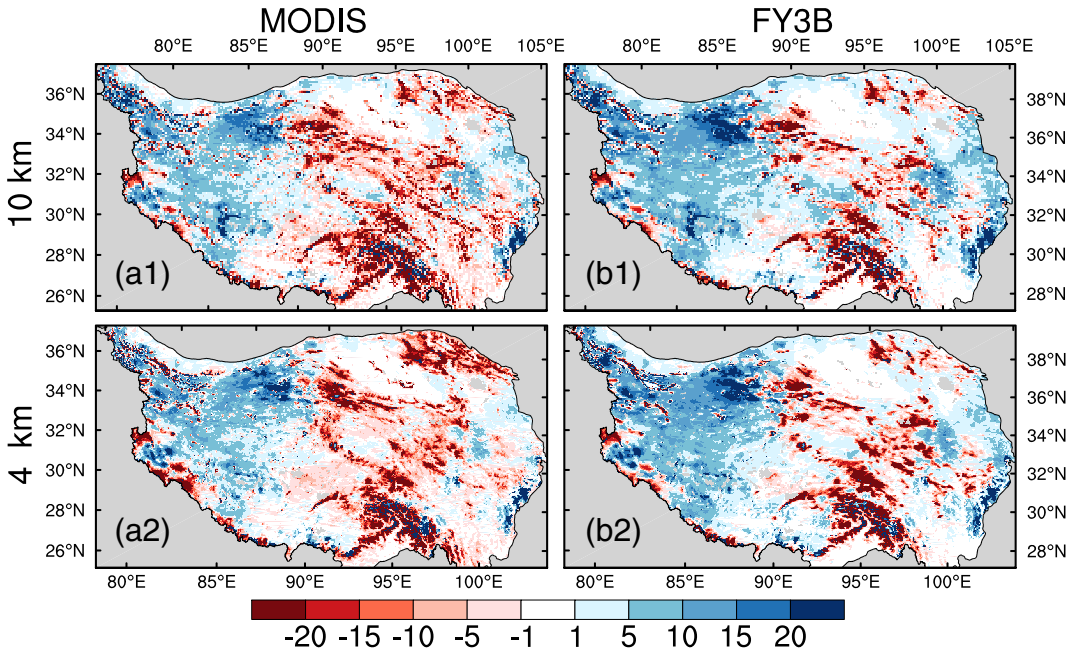

Figure 6. Annual-mean biases of SCF (%) from 1 September 2013 to 31 August 2014 between the MODIS/FY3B snow cover data and the simulation results of OPT/ON07 in 10- (a1–b1) and 4-km (a2–b2) resolutions, respectively.

4.4. Effects on Surface Energy Budget and Snow Depth

Uncertainty of SCF simulation will result in substantial uncertainty of land-atmosphere interactions by affecting the surface energy budget because of high snow albedo. Compared to the GLASS data, the CTL simulation significantly overestimates the surface albedo with biases over 0.1 for most areas of the TP (Figure 8a). The OPT simulation also has substantially higher surface albedo especially in the northwestern TP (Figure 8b), though its mean bias is reduced to around 0.08. Both the OPT/ON07 in 4- and 10-km resolutions produce similar and reasonable surface albedo with mean bias around 0.02. For different elevation bands, higher elevation has more significant improvements for the surface albedo during snow season, and the OPT simulation shows larger improvements than the optimized SCF schemes (Figures 9a1–9d1). Figures 9a1–9d1 also show that the biases of surface albedo in winter and spring are even lower than those in summer and autumn, which implies that the remaining albedo bias in the eastern TP may not be due to the uncertainty of snow cover.

The improvements of surface albedo substantially increase the winter net radiation fluxes of the OPT and the OPT/ON07 in 4- and 10-km simulations and the sensible and latent heat fluxes (Figures 9a2–9a4). In spring and autumn, only high elevation bands have higher net radiation and sensible heat for the improved SCF simulations, while latent heat does not change much. In general, sensible heat flux proportionally increases with the increased net radiation, indicating that the decreased albedo and SCF mainly result in increasing sensible heat. The latent heat fluxes of the OPT and OPT/ON07 in 4- and 10-km simulations are almost the same, so they are mainly affected by the OPT simulation.

Table 4
Seasonal and Annual Biases of SCF (%) Between the FY3B/MODIS Data and the Simulation Results of 4- and 10-km Resolutions, Respectively, Using the OPT With Optimized N07 Scheme (OPT/ON07) From 1 September 2013 to 31 August 2014

		Spring	Summer	Autumn	Winter	Annual
4 km	MODIS	−3.2	0.9	−1.5	1.4	−0.5
	FY3B	−0.1	3.0	−1.2	4.7	1.5
10 km	MODIS	−4.4	0.8	−2.2	2.2	−0.9
	FY3B	−0.3	2.6	1.3	5.1	2.1

Moreover, Figure 10a shows that the CTL simulation has a significant lower ground temperature (Tg) than in situ observations for most areas with mean biases around −3.5°C over the TP. Both the OPT and OPT/ON07 improve Tg substantially, with annual biases of Tg reducing to −1.2°C and −0.8°C, respectively, but effects of the optimizing SCF parametrizations on Tg are limited compared to those of the OPT (Figures 10b and 10c). This is because the OPT reduces the SCF by changing the option of surface exchange coefficient

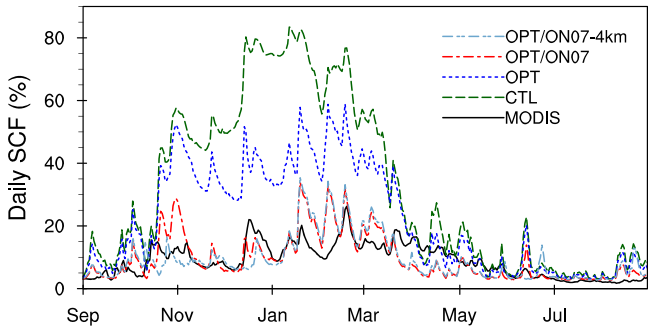

Figure 7. Spatial mean daily SCF from 1 September 2013 to 31 August 2014 for the MODIS SCF and the simulation results of the CTL, OPT, and OPT/ON07 in 10- and 4-km resolution.

process, while the optimized SCF parameterization reduces the SCF directly and the increased energy is mainly transferred to the atmosphere instead of warming up the ground (Figure 9). The OPT/ON07 in 4-km resolution simulation improves Tg in summer and autumn, reducing the annual bias to 0.5°C (supporting information Figure S4). In addition, negative bias of Tg could be found in the eastern TP where SCF is also underestimated for the OPT and OPT/ON07, because it is mainly from the underestimated air temperature (supporting information Figure S5) instead of the SCF bias itself. This also explains why the OPT/ON07 in the 4-km resolution with an adjusted air temperature shows better Tg in the eastern TP than that in the 10-km resolution.

Uncertainty of heat fluxes also affects the simulation of snow depth. Figure 11 shows that CTL has significantly higher snow depth in the TP, with annual mean biases of 4.2 mm compared to in situ observations. The OPT and OPT/ON07 improve snow depth substantially, with annual biases reduced to 1.3 and 0.2 mm, respectively (Figure 11). However, the OPT/ON07 in the 4-km resolution underestimates snow depth in fall and late spring when the snow cover is more sensitive to air temperature than that in winter.

5. Discussion

LSMs commonly have less optimal performance in complex and heterogeneous regions such as the TP. Therefore, we mainly focus on improving existing SCF parameterizations, optimizing parameters, and quantifying their contributions to seasonal snow simulations in this paper. This study provides a useful and effective method to update parameters, as parameter settings may depend on geographic location, climatology, and different versions of LSMs, which introduce uncertainties.

Atmospheric forcing conditions represent another uncertainty source of modeling snow cover (Chen et al., 2014; He et al., 2019; Mizukami et al., 2014). Clark et al. (2011) summarized that the watershed-scale snow cover is mainly shaped by meteorological data, which controls the freezing level

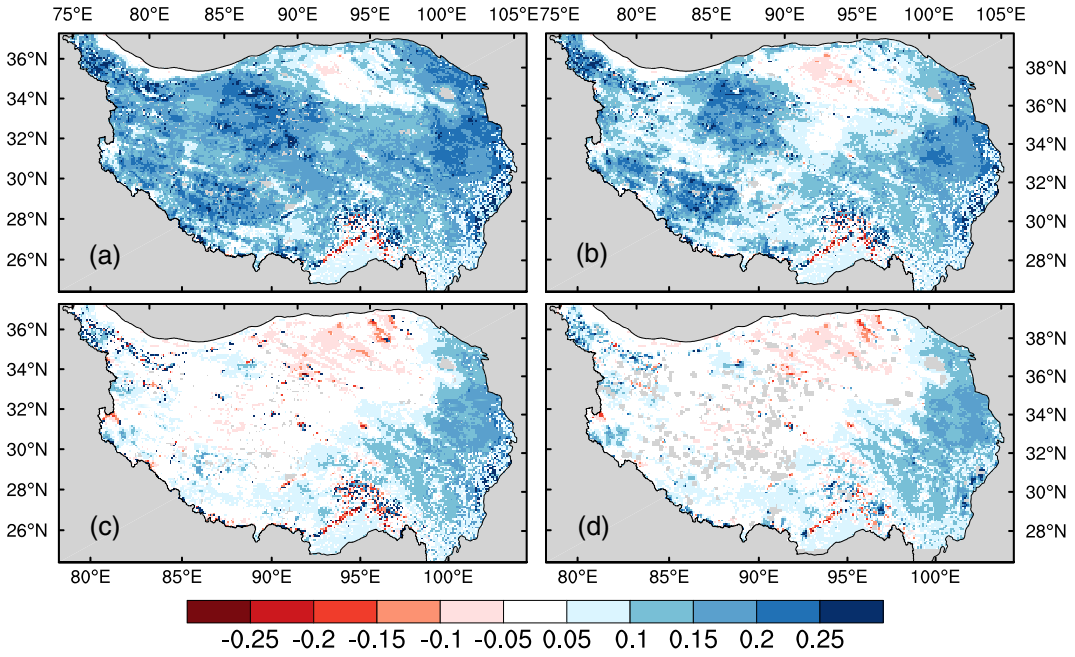

Figure 8. Mean biases of surface albedo from 1 September 2013 to 31 August 2014 of the simulation results of CTL (a), OPT (b), and OPT/ON07 in 10- (c) and 4-km (d) resolutions, with respect to the GLASS data.

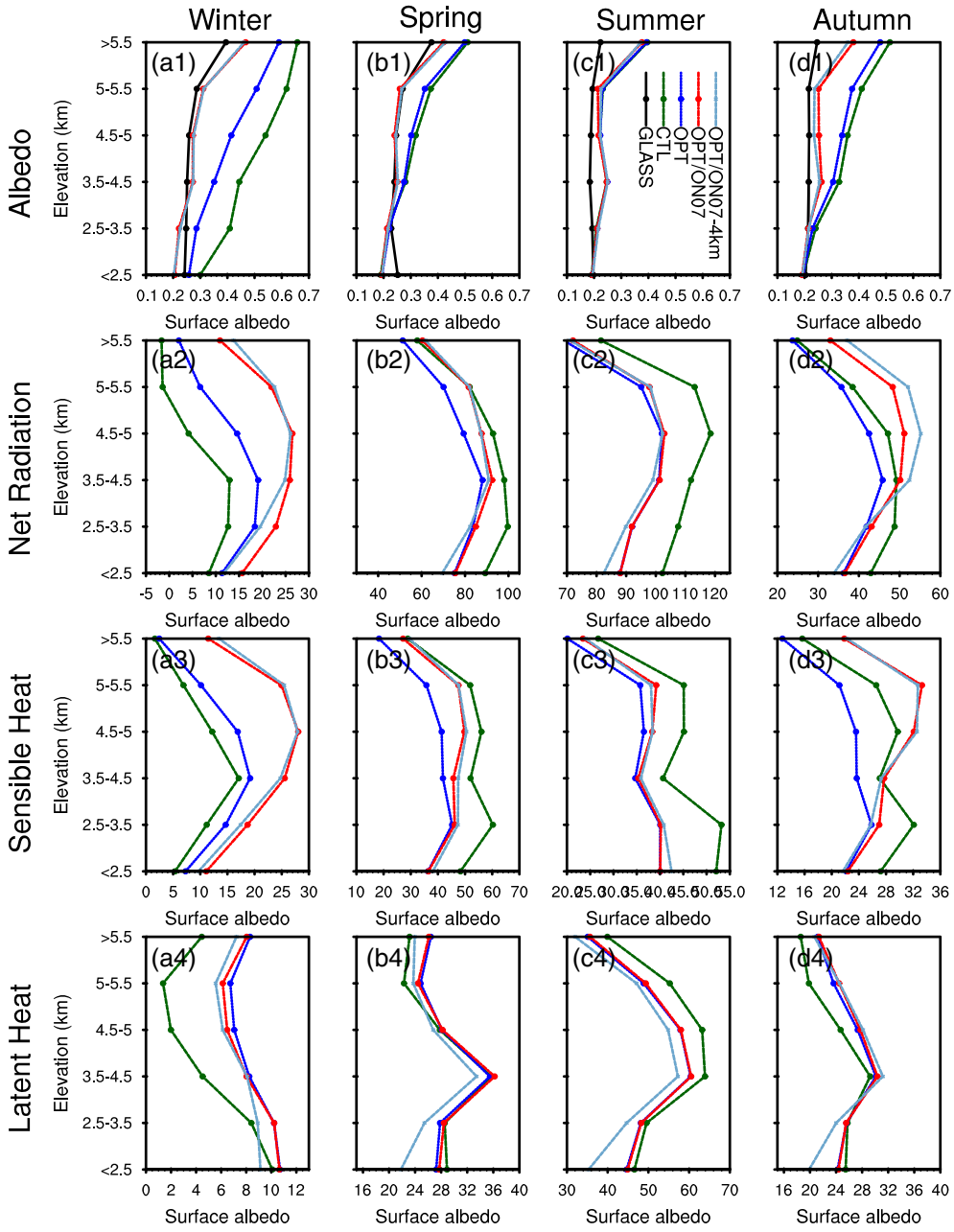

Figure 9. Seasonal-mean albedo, net radiation, sensible heat, and latent heat (W m^{-2}) averaged at six elevation zones (0–2.5, 2.5–3.5, 3.5–4.5, 4.5–5, 5–5.5, and >5.5 km) from 1 September 2013 to 31 August 2014 simulated by the CTL, OPT, and OPT with the optimized N07 scheme in 10-km resolution (OPT/ON07) and in 4-km resolution (OPT/ON07-4km), respectively.

and melt energy. Mizukami et al. (2014) and Raleigh et al. (2015) found that shortwave and longwave radiation significantly alter the snow melt timing, respectively. Chen et al. (2014) found that models performed better in SWE simulations with better atmospheric forcing data of precipitation and air temperature. A series of studies were applied to explore the impacts of precipitation data sets in different spatial resolutions produced by regional climate model on snowpack modeling over the French Mountains and found significant improvements of snow simulation with higher resolution precipitation data (Quéno et al., 2016; Vionnet et al., 2016, 2019). He et al. (2019) assessed the impacts of precipitation uncertainty on snowpack simulation in the western America using five precipitation data sets and found added values of convection-permitting

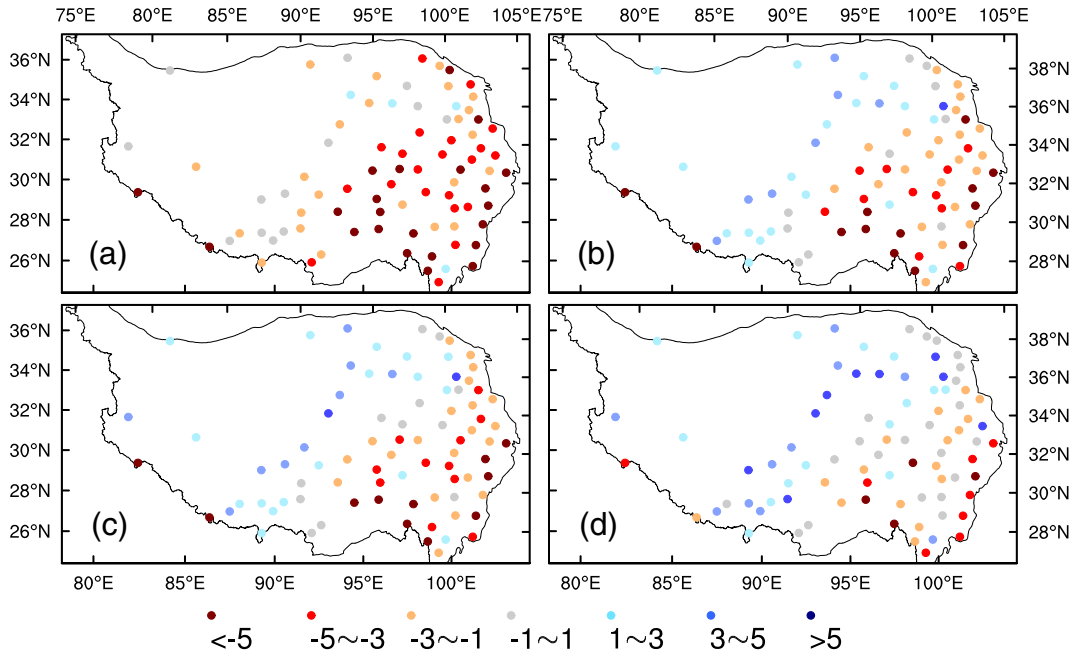

Figure 10. Biases of ground temperature (Tg; °C) from 1 September 2013 to 31 August 2014 of the nearest-grid simulation results of CTL (a), OPT (b), and OPT with the optimized N07 scheme in 10-km resolution (OPT/ON07; c) and in 4-km resolution (OPT/ON07-4km; d), respectively, with respect to the station observations in the TP.

modeling of precipitation for high-resolution snow simulations. Our recent findings in the TP agree with those of previous works and show that the underestimated SCF in the southeastern mountain regions of the TP can be improved significantly using a 4-km precipitation simulated by the WRF model (Gao et al., 2020). This suggests that the snow cover underestimate in other mountainous regions of the eastern TP is likely due to the underestimated topographic precipitation, and that if more accurate modeling/satellite precipitation data could be used to correct the forcing, the snow cover modeling would be improved.

Uncertainties in model physics schemes and parameters could lead to over 100% relative biases in SCF simulation. Some of these biases can be reduced efficiently using local observations through optimizing parameters as we showed in this study and through developing new schemes (Wang et al., 2020). Further uncertainty mitigation needs model physics improvements that consider the complex effect of topography. However, uncertainties of atmospheric forcing data on snow modeling are more complex and hard to be quantified, especially for areas with complex topography and insufficient observations. A main limitation of this work is that we do not have enough observations of atmospheric forcing data for an extensive analysis of uncertainty associated with the forcing data, especially in the mountains, which requires more in situ observations in the high mountains in the TP.

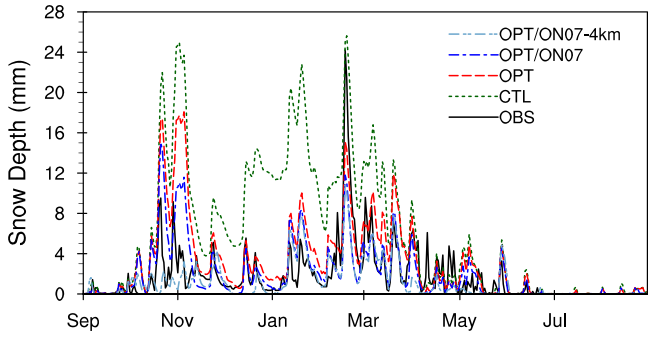

Figure 11. Daily snow depth (mm) from 1 September 2013 to 31 August 2014 for the station observations in the TP and the nearest-grid simulation results of CTL, OPT, and OPT with the optimized N07 scheme in 10-km resolution (OPT/ON07) and in 4-km resolution (OPT/ON07-4km), respectively.

Another limitation of this work is that we do not consider the impact and uncertainty of topography on model physics. The subgrid variation of topography is represented by the standard deviation of elevation here (supporting information Figure S6b), which shows that the complex topographic regions are mainly located near the boundaries and the southeastern TP, where SCF is underestimated. However, scatterplot of the standard deviation of elevation versus SCF biases (supporting information Figure S6c) does not show any significant correlation. This is probably due to the large study region over the whole TP and the rough spatial resolution used in this study,

because topographic effects on snow cover simulation highly rely on spatial resolution as discussed below.

On the mountain-range scale (usually from 1 km to less than 4 km in horizontal resolution), Mott et al. (2018) pointed out that snow depth distribution mainly attributes to topographic precipitation, which is consistent with studies using high-resolution convection-permitting regional climate models to produce precipitation for snow modeling (Gao et al., 2020; He et al., 2019; Quéno et al., 2016; Vionnet et al., 2016, 2019). At finer scales (usually several meters to less than 500 m), impacts of wind speed on snowfall sublimation and snowpack redistribution (drifting snow) are more significant. For example, Erickson et al. (2005) and Anderton et al. (2004) found that the most effective controller of snow redistribution is wind factor among several other terrain parameters including elevation, slope, and radiation. Impacts of topography on snow cover are considered using surface roughness (Barlage et al., 2010; Lehning et al., 2011) and 3-D mountain radiation with shadow effects (Fan et al., 2019) as well.

However, it is still not clear what should be the optimal spatial resolution for modeling topographic effects. A sensitivity test recommended a resolution of 250 m or less for a catchment in the High Atlas for snow modeling, because significant features of topography are smoothed out in coarse resolutions (Baba et al., 2019). This result may be not appropriate for other mountainous regions, but most of the above studies considering topographic effects used a resolution less than 1 km; none of them uses a resolution coarser than 3 km. Therefore, it is challenging to parameterize topographic effects for cross-scale applications.

6. Conclusions

In this study, we analyzed uncertainties in snow cover modeling over the TP associated with the Noah-MP multiple physics-scheme options, SCF parameterizations, and model spatial resolution. Our main conclusions are as follows.

Using the optimized Noah-MP physics-scheme options (OPT), we improved the SCF simulation significantly by reducing annual biases from 22.8% to 14.6% compared to the MODIS data and from 24.5% to 16.6% compared to the FY3B data. Optimizing the SCF parameterizations reduced annual SCF biases from around 15% to less than 2% for three of the five widely used parameterizations compared to the MODIS data. This indicates that the SCF parameterization is more important than the multiple physics-scheme options for reducing the uncertainty.

Compared to the 10-km simulation, the 4-km simulation with topographically adjusted air temperature showed slight improvements in annual and seasonal SCF but did not significantly improve the spatial distribution of SCF in mountainous areas. Thus, the uncertainty from using different model spatial resolutions seems limited in this study.

Reducing high biases of SCF led to significantly lower surface albedo, which was closer to the GLASS albedo. The lower surface albedo in turn resulted in higher net radiation flux and sensible heat flux. Consequently, simulations of surface temperature and snow depth were improved. The annual bias of surface temperature was reduced from −3.5°C to −0.8°C compared to that of CTL, and the bias of snow depth was reduced from 4.2 to 0.2 mm.

Data Availability Statement

Data used in this study are available through our previous work for the SCF satellite data sets of MODIS and FY-3B (Jiang et al., 2019) and the open access for the atmospheric forcing data (https://data.tpdc.ac.cn/zh-hans/data/8028b944-daaa-4511-8769-965612652c49/; He et al., 2020).

Acknowledgments

We thank Zhaojun Zheng and Jianduo Li from the National Satellite Meteorological Centre (NSMC) of CMA for helping with the usage of FY3B MULSS snow cover data. We also appreciate the free access of data sets from the National Meteorological Information Center of CMA and the National Snow and Ice Center (NSIDC). This research has been supported by the Second Tibetan Plateau Scientific Expedition and Research (STEP) program (2019QZKK010314), the National Natural Science Foundation of China (91537211 and 91537105), NOAA research grants NA18OAR4590398 and NA18OAR4310134, and the NCAR Water System. The National Center for Atmospheric Research is sponsored by the National Science Foundation. Support of the Fudan University-Tibet University Joint Laboratory for Biodiversity and Global Change is appreciated.

References

Anderton, S. P., White, S. M., & Alvera, B. (2004). Evaluation of spatial variability in snow water equivalent for a high mountain catchment. *Hydrological Processes*, *18*(3), 435–453. https://doi.org/10.1002/hyp.1319

Baba, M. W., Gascoin, S., Kinnard, C., Marchane, A., & Hanich, L. (2019). Effect of digital elevation model resolution on the simulation of the snow cover evolution in the High Atlas. *Water Resources Research*, *55*, 5360–5378. https://doi.org/10.1029/2018WR023789

Barlage, M., Chen, F., Tewari, M., Ikeda, K., Gochis, D., Dudhia, J., et al. (2010). Noah land surface model modifications to improve snowpack prediction in the Colorado Rocky Mountains. *Journal of Geophysical Research*, *115*, D22101. https://doi.org/10.1029/2009JD013470

Barlage, M., Tewari, M., Chen, F., Miguez-Macho, G., Yang, Z.-L., & Niu, G.-Y. (2015). The effect of groundwater interaction in North American regional climate simulations with WRF/Noah-MP. *Climatic Change*, *129*(3–4), 485–498. https://doi.org/10.1007/s10584-014-1308-8

Birkhoff, G., & De Boor, C. R. (1965). Piecewise polynomial interpolation and approximation. *Approximation of functions* (pp. 164–190). Amsterdam: Elsevier Publ. Co.

Chen, F., Barlage, M., Tewari, M., Rasmussen, R., Jin, J., Lettenmaier, D., et al. (2014). Modeling seasonal snowpack evolution in the complex terrain and forested Colorado Headwaters region: A model intercomparison study. *Journal of Geophysical Research*, *119*, 13,795–13,819. https://doi.org/10.1002/2014JD022167

Chen, F., Manning, K. W., Lemone, M. A., Trier, S. B., Alfieri, J. G., Roberts, R., et al. (2007). Description and evaluation of the characteristics of the NCAR high-resolution land data assimilation system. *Journal of Applied Meteorology and Climatology*, *46*(6), 694–713. https://doi.org/10.1175/JAM2463.1

Clark, M. P., & Serreze, M. C. (2000). Effects of variations in East Asian snow cover on modulating atmospheric circulation over the North Pacific Ocean. *Journal of Climate*, *13*(20), 3700–3710. https://doi.org/10.1175/1520-0442(2000)013<3700:EOVIEA>2.0.CO;2

Clark, M. P., Hendrikx, J., Slater, A. G., Kavetski, D., Anderson, B., Cullen, N. J., et al. (2011). Representing spatial variability of snow water equivalent in hydrologic and land-surface models: A review. *Water Resources Research*, *47*, W07539. https://doi.org/10.1029/2011WR010745

Dai, Y., Shangguan, W., Duan, Q., Liu, B., Fu, S., & Niu, G. (2013). Development of a China dataset of soil hydraulic parameters using pedotransfer functions for land surface modeling. *Journal of Hydrometeorology*, *14*(3), 869–887. https://doi.org/10.1175/jhm-d-12-0149.1

Dickinson, E., Henderson-Sellers, A., Kennedy, J., & Wilson, M. F. (1986). *Biosphere-Atmosphere Transfer Scheme (BATS) for the NCAR community climate model, NCAR Tech. Note NCAR/TN- 275+STR*. USA: NCAR. https://opensky.ucar.edu/islandora/object/technotes:383

Dong, C., Yang, J., Zhang, W., Yang, Z., Lu, N., Shi, J., et al. (2009). An overview of a new Chinese weather satellite FY-3A. *Bulletin of the American Meteorological Society*, *90*(10), 1531–1544. https://doi.org/10.1175/2009BAMS2798.1

Donville, H., Royer, J.-F., & Mahfouf, J.-F. (1995). A new snow parameterization for the Météo-France climate model, Part I: Validation in stand-alone experiments. *Climate Dynamics*, *35*, 21–35. https://doi.org/10.1007/BF00208761

Erickson, T. A., Williams, M. W., & Winstral, A. (2005). Persistence of topographic controls on the spatial distribution of snow in rugged mountain terrain, Colorado, United States. *Water Resources Research*, *41*, 1–17. https://doi.org/10.1029/2003WR002973

Fan, X., Gu, Y., Liou, K. N., Lee, W. L., Zhao, B., Chen, H., & Lu, D. (2019). Modeling study of the impact of complex terrain on the surface energy and hydrology over the Tibetan Plateau. *Climate Dynamics*, *53*(11), 6919–6932. https://doi.org/10.1007/s00382-019-04966-z

Gao, Y., & Chen, D. (2017). Modeling of regional climate over the Tibetan Plateau. *Oxford research encyclopedia of climate science* (February 2018, pp. 1–29). New York: Oxford University Press.

Gao, Y., Chen, F., & Jiang, Y. (2020). Evaluation of a convection-permitting modeling of precipitation over the Tibetan Plateau and its influences on the simulation of snow-cover fraction. *Journal of Hydrometeorology*, *21*(7), 1531–1548. https://doi.org/10.1175/JHM-D-19-0277.1

Gao, Y., Chen, F., Lettenmaier, D. P., Xu, J., Xiao, L., & Li, X. (2018). Does elevation-dependent warming hold true above 5000 m elevation? Lessons from the Tibetan Plateau. *npj Climate and Atmospheric Science*, *1*(1), 19. https://doi.org/10.1038/s41612-018-0030-z

Gao, Y., Li, K., Chen, F., Jiang, Y., & Lu, C. (2015). Assessing and improving Noah-MP land model simulations for the central Tibetan Plateau. *Journal of Geophysical Research: Atmospheres*, *120*, 9258–9278. https://doi.org/10.1002/2015JD023404

Gao, Y., Xiao, L., Chen, D., Chen, F., Xu, J., & Xu, Y. (2016). Quantification of the relative role of land-surface processes and large-scale forcing in dynamic downscaling over the Tibetan Plateau. *Climate Dynamics*, *48*(5-6), 1705–1721. https://doi.org/10.1007/s00382-016-3168-6

Gao, Y., Xu, J., & Chen, D. (2015). Evaluation of WRF mesoscale climate simulations over the Tibetan Plateau during 1979–2011. *Journal of Climate*, *28*(7), 2823–2841. https://doi.org/10.1175/JCLI-D-14-00300.1

Hall D. K., Riggs G. A., Salomonson V. V., DiGirolamo N. E., & Bayr K. J. (2002). MODIS snow-cover products. *Remote Sensing of Environment*, *83*(1–2), 181–194. https://doi.org/10.1016/s0034-4257(02)00095-0

He, C., Chen, F., Barlage, M., Liu, C., Newman, A., Tang, W., et al. (2019). Can convection-permitting modeling provide decent precipitation for offline high-resolution snowpack simulations over mountains? *Journal of Geophysical Research: Atmospheres*, *124*, 12,631–12,654. https://doi.org/10.1029/2019JD030823

He, J., Yang, K., Tang, W., Lu, H., Qin, J., Chen, Y., & Li, X. (2020). The first high-resolution meteorological forcing dataset for land process studies over China. *Scientific Data*, *7*(1), 25–11. https://doi.org/10.1038/s41597-020-0369-y

Immerzeel, W. W., van Beek, L. P. H., & Bierkens, M. F. P. (2010). Climate change will affect the Asian water towers. *Science*, *328*(5984), 1382–1385. https://doi.org/10.1126/science.1183188

Jiang, Y., Chen, F., Gao, Y., Barlage, M., & Li, J. (2019). Using multisource satellite data to assess recent snow-cover variability and uncertainty in the Qinghai–Tibet Plateau. *Journal of Hydrometeorology*, *20*(7), 1293–1306. https://doi.org/10.1175/jhm-d-18-0220.1

Jiang, Y., Gao, Y., Dong, Z., Liu, B., & Zhao, L. (2018). Simulations of wind erosion along the Qinghai-Tibet Railway in north-central Tibet. *Aeolian Research*, *32*, 192–201. https://doi.org/10.1016/j.aeolia.2018.03.006

Kang, S., Xu, Y., You, Q., Flügel, W. A., Pepin, N., & Yao, T. (2010). Review of climate and cryospheric change in the Tibetan Plateau. *Environmental Research Letters*, *5*(1), 015101. https://doi.org/10.1088/1748-9326/5/1/015101

Lehning, M., Grünewald, T., & Schirmer, M. (2011). Mountain snow distribution governed by an altitudinal gradient and terrain roughness. *Geophysical Research Letters*, *38*, 1–5. https://doi.org/10.1029/2011GL048927

Lewis, P., & Barnsley, M. (1994). Influence of the sky radiance distribution on various formulations of the earth surface albedo. In *Proceedings of the conference on physical measurements and signatures in remote sensing* (707–715). France: Val d'Isere. Retrieved from http://www2.geog.ucl.ac.uk/~plewis/LewisBarnsley1994.pdf

Li, G., Wang, Z. S., & Huang, N. (2018). A snow distribution model based on snowfall and snow drifting simulations in mountain area. *Journal of Geophysical Research: Atmospheres*, *123*, 7193–7203. https://doi.org/10.1029/2018JD028434

Li, J., Chen, F., Zhang, G., Barlage, M., Gan, Y., Xin, Y., & Wang, C. (2018). Impacts of land cover and soil texture uncertainty on land model simulations over the central Tibetan Plateau. *Journal of Advances in Modeling Earth Systems*, *10*(9), 2121–2146. https://doi.org/10.1029/2018MS001377

Liston, G. E. (2004). Representing subgrid snow cover heterogeneities in regional and global models. *Journal of Climate*, *17*(6), 1381–1397. https://doi.org/10.1175/1520-0442(2004)017<1381:RSSCHI>2.0.CO;2

Liu, X., & Yanai, M. (2002). Influence of Eurasian spring snow cover on Asian summer rainfall. *International Journal of Climatology*, *22*(9), 1075–1089. https://doi.org/10.1002/joc.784

Livneh, B., Xia, Y., Mitchell, K. E., Ek, M. B., & Lettenmaier, D. P. (2010). Noah LSM snow model diagnostics and enhancements. *Journal of Hydrometeorology*, *11*(3), 721–738. https://doi.org/10.1175/2009JHM1174.1

Luce, C. H., Tarboton, D. G., & Cooley, K. R. (1999). Sub-grid parameterization of snow distribution for an energy and mass balance snow cover model. *Hydrological Processes*, *13*(12–13), 1921–1933. https://doi.org/10.1002/(SICI)1099-1085(199909)13:12/13<1921::AID-HYP867>3.0.CO;2-S

Lucht, W., Schaaf, C. B., & Strahler, A. H. (2000). An algorithm for the retrieval of albedo from space using semiempirical BRDF models. *IEEE Transactions on Geoscience and Remote Sensing*, *38*(2 II), 977–998. https://doi.org/10.1109/36.841980

Ma, N., Niu, G. Y., Xia, Y., Cai, X., Zhang, Y., Ma, Y., & Fang, Y. (2017). A systematic evaluation of Noah-MP in simulating land-atmosphere energy, water, and carbon exchanges over the continental United States. *Journal of Geophysical Research: Atmospheres*, *122*, 12,245–12,268. https://doi.org/10.1002/2017JD027597

Ma, N., Szilagyi, J., Zhang, Y., & Liu, W. (2019). Complementary-relationship-based modeling of terrestrial evapotranspiration across China during 1982–2012: Validations and spatiotemporal analyses. *Journal of Geophysical Research: Atmospheres*, *124*, 4326–4351. https://doi.org/10.1029/2018JD029850

Minder, J. R., Letcher, T. W., & Skiles, S. M. K. (2016). An evaluation of high-resolution regional climate model simulations of snow cover and albedo over the Rocky Mountains, with implications for the simulated snow-albedo feedback. *Journal of Geophysical Research: Atmospheres*, *121*, 9069–9088. https://doi.org/10.1002/2016JD024995

Mizukami, N., Clark, M. P., Slater, A. G., Brekke, L. D., Elsner, M. M., Gangopadhyay, S., & Arnold, J. R. (2014). Hydrologic implications of different large-scale meteorological model forcing datasets in mountainous regions. *Journal of Hydrometeorology*, *15*(1), 474–488. https://doi.org/10.1175/JHM-D-13-036.1

Mott, R., Vionnet, V., & Grünewald, T. (2018). The seasonal snow cover dynamics: Review on wind-driven coupling processes. *Frontiers in Earth Science*, *6*. https://doi.org/10.3389/feart.2018.00197

Niu, G. Y., & Yang, Z. L. (2007). An observation-based formulation of snow cover fraction and its evaluation over large North American river basins. *Journal of Geophysical Research*, *112*, D21101. https://doi.org/10.1029/2007JD008674

Niu, G.-Y., Yang, Z.-L., Mitchell, K. E., Chen, F., Ek, M. B., Barlage, M., et al. (2011). The community Noah land surface model with multiparameterization options (Noah-MP): 1 Model description and evaluation with local-scale measurements. *Journal of Geophysical Research*, *116*, D12109. https://doi.org/10.1029/2010JD015139

Orsolini, Y., Wegmann, M., Dutra, E., Liu, B., Balsamo, G., Yang, K., et al. (2019). Evaluation of snow depth and snow cover over the Tibetan Plateau in global reanalyses using in situ and satellite remote sensing observations. *The Cryosphere*, *13*(8), 2221–2239. https://doi.org/10.5194/tc-13-2221-2019

Quéno, L., Vionnet, V., Dombrowski-Etchevers, I., Lafaysse, M., Dumont, M., & Karbou, F. (2016). Snowpack modelling in the Pyrenees driven by kilometric-resolution meteorological forecasts. *The Cryosphere*, *10*(4), 1571–1589. https://doi.org/10.5194/tc-10-1571-2016

Raleigh, M. S., Livneh, B., Lapo, K., & Lundquist, J. D. (2015). How does availability of meteorological forcing data impact physically based snowpack simulations? *Journal of Hydrometeorology*, *17*(1), 99–120. https://doi.org/10.1175/jhm-d-14-0235.1

Roesch, A., Wild, M., Gilgen, H., & Ohmura, A. (2001). A new snow cover fraction parameterization for the ECHAM4 GCM. *Climate Dynamics*, *17*(12), 933–946. https://doi.org/10.1007/s003820100153

Romanov, P., & Tarpley, D. (2004). Estimation of snow depth over open prairie environments using GOES imager observations. *Hydrological Processes*, *18*(6), 1073–1087. https://doi.org/10.1002/hyp.5508

Steger, C., Kotlarski, S., Jonas, T., & Schär, C. (2013). Alpine snow cover in a changing climate: A regional climate model perspective. *Climate Dynamics*, *41*(3–4), 735–754. https://doi.org/10.1007/s00382-012-1545-3

Swenson, S. C., & Lawrence, D. M. (2012). A new fractional snow-covered area parameterization for the Community Land Model and its effect on the surface energy balance. *Journal of Geophysical Research*, *117*, D21107. https://doi.org/10.1029/2012JD018178

Toure, A. M., Rodell, M., Yang, Z.-L., Beaudoing, H., Kim, E., Zhang, Y., & Kwon, Y. (2016). Evaluation of the snow simulations from the Community Land Model, version 4 (CLM4). *Journal of Hydrometeorology*, *17*(1), 153–170. https://doi.org/10.1175/JHM-D-14-0165.1

Vernekar, A. D., Zhou, J., & Shukla, J. (1995). The effect of Eurasian snow cover on the Indian monsoon. *Journal of Climate*, *8*(2), 248–266. https://doi.org/10.1175/1520-0442(1995)008<0248:TEOESC>2.0.CO;2

Vionnet, V., Dombrowski-Etchevers, I., Lafaysse, M., Quéno, L., Seity, Y., & Bazile, E. (2016). Numerical weather forecasts at kilometer scale in the French Alps: Evaluation and application for snowpack modeling. *Journal of Hydrometeorology*, *17*(10), 2591–2614. https://doi.org/10.1175/JHM-D-15-0241.1

Vionnet, V., Six, D., Auger, L., Dumont, M., Lafaysse, M., Quéno, L., et al. (2019). Sub-kilometer precipitation datasets for snowpack and glacier modeling in alpine terrain. *Frontiers in Earth Science*, *7*, 1–21. https://doi.org/10.3389/feart.2019.00182

Wang, W., Yang, K., Zhao, L., Zheng, Z., Lu, H., Mamtimin, A., et al. (2020). Characterizing surface albedo of shallow fresh snow and its importance for snow ablation on the interior of the Tibetan Plateau. *Journal of Hydrometeorology*, *21*(4), 815–827. https://doi.org/10.1175/jhm-d-19-0193.1

Wang, Z., Wu, R., Chen, S., Huang, G., Liu, G., & Zhu, L. (2018). Influence of western Tibetan Plateau summer snow cover on East Asian summer rainfall. *Journal of Geophysical Research: Atmospheres*, *123*, 2371–2386. https://doi.org/10.1002/2017JD028016

Wang, Z., Zeng, X., Barlage, M., Dickinson, R. E., Gao, F., & Schaaf, C. B. (2004). Using MODIS BRDF and albedo data to evaluate global model land surface albedo. *Journal of Hydrometeorology*, *5*(1), 3–14. https://doi.org/10.1175/1525-7541(2004)005<0003:UMBAAD>2.0.CO;2

Wu, G., Liu, Y., He, B., Bao, Q., Duan, A., & Jin, F. F. (2012). Thermal controls on the Asian summer monsoon. *Scientific Reports*, *2*, 404. https://doi.org/10.1038/srep00404

Wu, G., Liu, Y., Zhang, Q., Duan, A., Wang, T., Wan, R., et al. (2007). The influence of mechanical and thermal forcing by the Tibetan Plateau on Asian climate. *Journal of Hydrometeorology*, *8*(4), 770–789. https://doi.org/10.1175/JHM609.1

Wu, T.-W., & Qian, Z.-A. (2003). The relation between the Tibetan winter snow and the Asian summer monsoon and rainfall: An observational investigation. *Journal of Climate*, *16*(12), 2038–2051. https://doi.org/10.1175/1520-0442(2003)016<2038:TRBTTW>2.0.CO;2

Xia, K., Wang, B., Li, L., Shen, S., Huang, W., Xu, S., et al. (2014). Evaluation of snow depth and snow cover fraction simulated by two versions of the flexible global ocean-atmosphere-land system model. *Advances in Atmospheric Sciences*, *31*(2), 407–420. https://doi.org/10.1007/s00376-013-3026-y

Xie, Z. Z., Hu, Z., Xie, Z. Z., Jia, B., Sun, G., Du, Y., & Song, H. (2018). Impact of the snow cover scheme on snow distribution and energy budget modeling over the Tibetan Plateau. *Theoretical and Applied Climatology*, *131*(3–4), 951–965. https://doi.org/10.1007/s00704-016-2020-6

Xu, L., & Dirmeyer, P. (2011). Snow-atmosphere coupling strength in a global atmospheric model. *Geophysical Research Letters*, *38*, 1–5. https://doi.org/10.1029/2011GL048049

Xue, Y. (2003). Impact of parameterizations in snow physics and interface processes on the simulation of snow cover and runoff at several cold region sites. *Journal of Geophysical Research*, *108*(D22), 8859. https://doi.org/10.1029/2002JD003174

Yang, Z., Niu, G., Mitchell, K. E., Chen, F., Ek, M. B., Barlage, M., et al. (2011). The community Noah land surface model with multiparameterization options (Noah-MP): 2 Evaluation over global river basins. *Journal of Geophysical Research*, *116*, D12110. https://doi.org/10.1029/2010JD015140

Yang, Z. L., Dickinson, R. E., Robock, A., & Vinnikov, K. Y. (1997). Validation of the snow submodel of the biosphere-atmosphere transfer scheme with Russian snow cover and meteorological observational data. *Journal of Climate*, *10*(2), 353–373. https://doi.org/10.1175/1520-0442(1997)010<0353:VOTSSO>2.0.CO;2

Yao, T., Xue, Y., Chen, D., Chen, F., Thompson, L., Cui, P., et al. (2019). Recent third pole's rapid warming accompanies cryospheric melt and water cycle intensification and interactions between monsoon and environment: Multidisciplinary approach with observations, modeling, and analysis. *Bulletin of the American Meteorological Society*, *100*(3), 423–444. https://doi.org/10.1175/BAMS-D-17-0057.1

You, Y., Huang, C., Gu, J., Li, H., Hao, X., & Hou, J. (2020). Assessing snow simulation performance of typical combination schemes within Noah-MP in northern Xinjiang, China. *Journal of Hydrology*, *581*, 124380. https://doi.org/10.1016/j.jhydrol.2019.124380

Zhang, G., Chen, F., & Gan, Y. (2016). Assessing uncertainties in the Noah-MP ensemble simulations of a cropland site during the Tibet Joint International Cooperation program field campaign. *Journal of Geophysical Research: Atmospheres*, *121*, 9576–9596. https://doi.org/10.1002/2016JD024928

Zhang, Y., Li, T., & Wang, B. (2004). Decadal change of the spring snow depth over the Tibetan Plateau: The associated circulation and influence on the East Asian summer monsoon*. *Journal of Climate*, *17*(14), 2780–2793. https://doi.org/10.1175/1520-0442(2004)017<2780:DCOTSS>2.0.CO;2